

06,13

Characteristic of the $\text{Ba}_{0.8}\text{Sr}_{0.2}\text{TiO}_3$ film interface with the Si (100) surface

© A.T. Kozakov¹, A.V. Nikolskiy¹, V.M. Mukhortov², Yu.I. Golovko², A.A. Skriabin¹, D.V. Stryukov²¹ Scientific Research Institute of Physics, Southern Federal University, Rostov-on-Don, Russia² Southern Scientific Center of Russian Academy of Sciences, Rostov-on-Don, Russia

E-mail: kozakov_a@mail.ru

Received October 2, 2023

Revised October 2, 2023

Accepted October 10, 2023

Using X-ray photoelectron spectroscopy, the chemical bonds at the interface between the single-crystal surface of a silicon substrate (p- and n-type) and the $\text{Ba}_{0.8}\text{Sr}_{0.2}\text{TiO}_3$ (BST) film of Si(100)/ $\text{Ba}_{0.8}\text{Sr}_{0.2}\text{TiO}_3$ heterostructures, which were created by sputtering ceramic $\text{Ba}_{0.8}\text{Sr}_{0.2}\text{TiO}_3$ targets in a high-frequency γ -discharge at elevated oxygen pressure (~ 1 Torr) using the „Plasma 50 SE“ unit. Chemical bonds at the interface between the single-crystal surface of a silicon substrate (p- and n-type) and the $\text{Ba}_{0.8}\text{Sr}_{0.2}\text{TiO}_3$ (BST) film of Si(100)/ $\text{Ba}_{0.8}\text{Sr}_{0.2}\text{TiO}_3$ heterostructures have been studied using X-ray photoelectron spectroscopy. Heterostructures were created by sputtering a $\text{Ba}_{0.8}\text{Sr}_{0.2}\text{TiO}_3$ ceramic target in a high-frequency γ -discharge at a sufficiently high oxygen pressure (~ 1 Torr) on the „Plasma 50 SE“ installation of two orientations of crystallites in the films: [001] and [011]. The bulk fraction of BST crystallites with [001] orientation is 96% for the n-type Si substrate and 97% for the p-type Si substrate. The bulk fraction of BST crystallites with [011] orientation is 4% for the n-type Si substrate and 3% for the p-type Si substrate. X-ray electron studies have shown that 46% of the silicon atoms at the interface are bound to oxygen, belonging to the BST structure; 18% of silicon atoms belong to the SiO_2 layer. In addition, at the interface there are titanium and strontium atoms chemically bonded to the silicon atoms and oxygen atoms of the BST structure. The Si/BST interface is sharp and at a thickness of ~ 6 Å is already fully formed.

Keywords: X-ray photoelectron spectroscopy, chemical bonds, interface, surface, silicon substrate, crystallites.

DOI: 10.61011/PSS.2023.11.57324.217

1. Introduction

Barium strontium titanate ($\text{Ba}_{1-x}\text{Sr}_x\text{TiO}_3$, BST) has a high dielectric constant, a low dielectric loss, and a low leakage current density [1,2]. Heterostructures based on it are an active medium for the manufacture of electrically tunable microwave and EHF devices (phased antenna arrays, tunable resonators, filters, delay lines) with low energy consumption in control circuits [3–10]; ultrafast optical modulators [5]; non-volatile memory, etc.

Silicon is planned to be used as a substrate in many devices using ferroelectric films. However, from experimental data it follows that during the formation of a ferroelectric film, chemical compounds are formed at the film-silicon interface. For example, according to [11], when BST films were deposited on pure silicon, an interface layer with a thickness of 30 Å was formed with intermediate values of the static dielectric constant ($K \sim 12$) and refraction index ($n \sim 2.6$ for photons with an energy of 1.5–3.25 eV). In [12], using high-resolution electron microscopy (HREM) it was found that an amorphous layer with a thickness of ≈ 5.0 nm and titanium disilicide is formed at the interface between BST and Si. On the other hand, in the case of depositing SrTiO_3 on n-type Si (001), the data of photoelectron emission, electron diffraction [13], scanning electron microscopy [14] and transmission electron microscopy [15] indicate a sharp boundary and the absence

of chemical reactions at the interface. Models of the Si/SrTiO₃ interface structure proposed in [14,15] can be useful for understanding the structure of the Si/BST system interface, provided that some of the strontium atoms in them are replaced by barium atoms. However, the research methods used in [14,15] do not allow understanding the chemical bonds at the Si/SrTiO₃ interface; in particular, the role of oxygen in its formation remains unclear.

Therefore, this study is focused on investigating the chemical state of atoms at the interface between the single-crystal surface of a silicon substrate and the $\text{Ba}_{0.8}\text{Sr}_{0.2}\text{TiO}_3$ (BST) film using X-ray photoelectron spectroscopy.

2. Experiment

2.1. Fabricating the $\text{Ba}_{0.8}\text{Sr}_{0.2}\text{TiO}_3/\text{Si}$ heterostructure

To fabricate heterostructures, we used the method we developed for the deposition [16,17] of ferroelectric complex oxides, which is used in the „Plasma 50 SE“ setup. The difference between the proposed high-frequency deposition of ferroelectric oxides and known analogues is that the growth of films occurs from the dispersed phase of the oxide formed in the plasma of a high-current (> 100 W/cm²) high-frequency γ -discharge when sputtering a ceramic target under high oxygen pressures (~ 1 Torr) at the cluster level

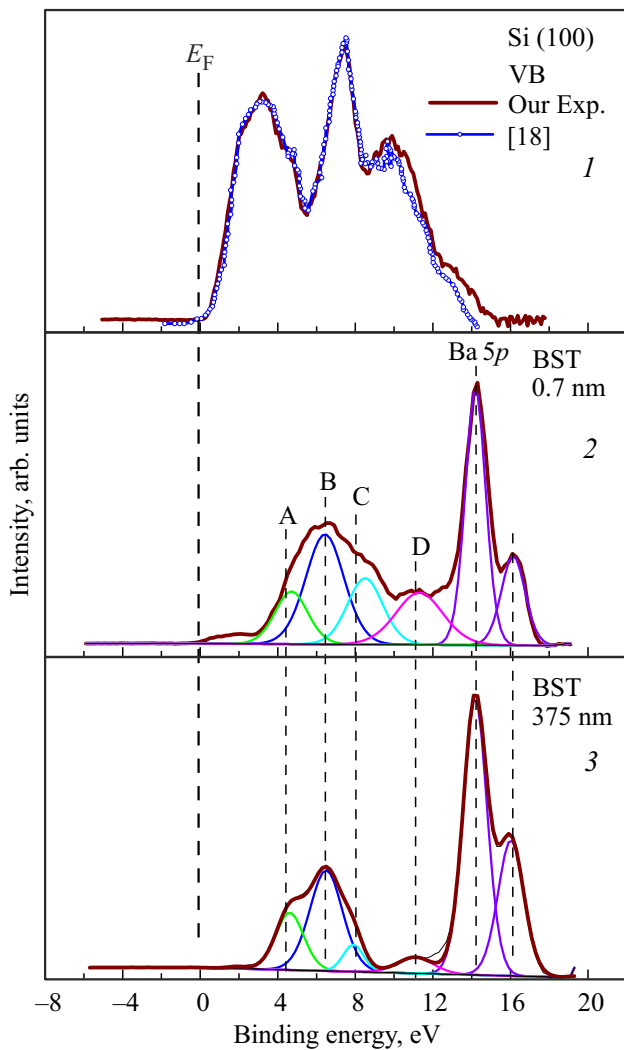


Figure 1. X-ray photoelectron spectra of the valence band of the Si(100) surface cleaned in HF (brown color — our experiment) and the spectrum of the valence band of the single-crystal Si(100) surface produced by the authors of [18] (panel 1). The spectra on panels 2 and 3 refer to BST films with thicknesses of 0.7 and 375 nm, respectively.

with their subsequent growth to plasma condensate. The growth mechanisms, the degree of structural perfection, and thus the properties of films can be varied widely, being within the framework of three-dimensional phase space q, p, b , where q is degree of structural perfection of the film, p is oxygen pressure, b is generalized parameter of the energy state of the condensate, which is determined on the basis of spatial optical emission spectroscopy [16].

The target used was $Ba_{0.8}Sr_{0.2}TiO_3$ (BST08) ceramics with tetragonal lattice constants of $a = 0.3937$ nm, $c = 0.3997$ nm. Two series of BST films with thicknesses from 0.7 to 375 nm on single-crystal Si substrates of n-type and p-type conductivities were produced and studied.

Preparation of silicon substrates before deposition included removal of the oxide layer in fluoric acid (5 min) followed by washing in deionized water and drying with dry

nitrogen. To monitor the state of the cleaned surface, X-ray photoelectron spectra of the valence band and spectra of the main Si2p-levels were recorded. Figure 1 (panel 1) shows the spectra of the valence band of the cleaned surface, and panels 2 and 3 show the X-ray photoelectron spectra of the valence bands of the films illustrating the change in the fine structure of the valence band with increasing the thickness of the BST layer deposited on the silicon surface.

As is known [18,19], the X-ray photoelectron spectra of the valence band of single-crystal Si have a specific shape, shown in panel 1 (Figure 1), and are radically different in fine structure from the spectra of the valence band of amorphous silicon. Therefore, from the comparison of two profiles of valence spectra in Figure 1 (panel 1), recorded by us and the authors of [18], a conclusion can be made that the surface of cleaned silicon was single-crystal. Spectroscopy data of the main Si2p-levels indicated that it contained a thin film (several tenths of nanometer) of SiO_2 and traces of fluoric acid. The comparison of the spectrum in Figure 1 (panel 3) with experiment and calculated data [20,21] shows that it refers to the BST film and is mainly represented by valence states of oxygen [21].

2.2. X-ray diffraction of BST films

The structural perfection of the film and the lattice cell parameters in the direction normal to the plane at room temperature were studied using a DRON-4-07 diffractometer ($\Theta-2\Theta$ -method). Figure 2, *a* and *b* show X-ray diffraction patterns of the studied Si(p)/BST and Si(n)/BST samples with thicknesses of 300 and 375 nm, respectively. In the diffraction patterns in the 2θ angle range from 20 up to 50° of both BST08/Si films (n-type) and BST08/Si films (p-type) there are only (001), (011), and (002) reflections from BST08, which is indicative of the presence of texture in the films, and the [001] and [011] directions are perpendicular to the substrate plane. The volume percentage of BST crystallites with the [001] orientation is 96% for the Si (n-type) substrate and 97% for the Si (p-type) substrate. The volume percentage of BST crystallites with the [011] orientation is 4% for the n-type Si substrate and 3% for the p-type Si substrate. Reflections of impurity phases are not detected in both diffraction patterns. From the analysis of the angular positions of the (002) lines, the parameters of BST lattice cells along the direction of the normal to the substrate surface were determined: $c = 0.4040$ nm for n-type Si and $c = 0.4044$ nm for p-type Si. Compared to the bulk material, the lattice constants for both the film on the n-type Si substrate and the film on the p-type Si substrate are increased; therefore, in these layers there are compressive stresses in the plane of the substrate.

The X-ray diffraction pattern of a Si/BST08 film with a thickness of 50 nm is shown in Figure 2, *c*. The diffraction pattern in the 2θ angle range from 20 to 50° contains (001), (011), and (002) reflections from BST, and the (011) reflection has an intensity comparable with those of (001) and (002) reflections, which is indicative of the presence of texture in the films, and the [001] and [011] directions

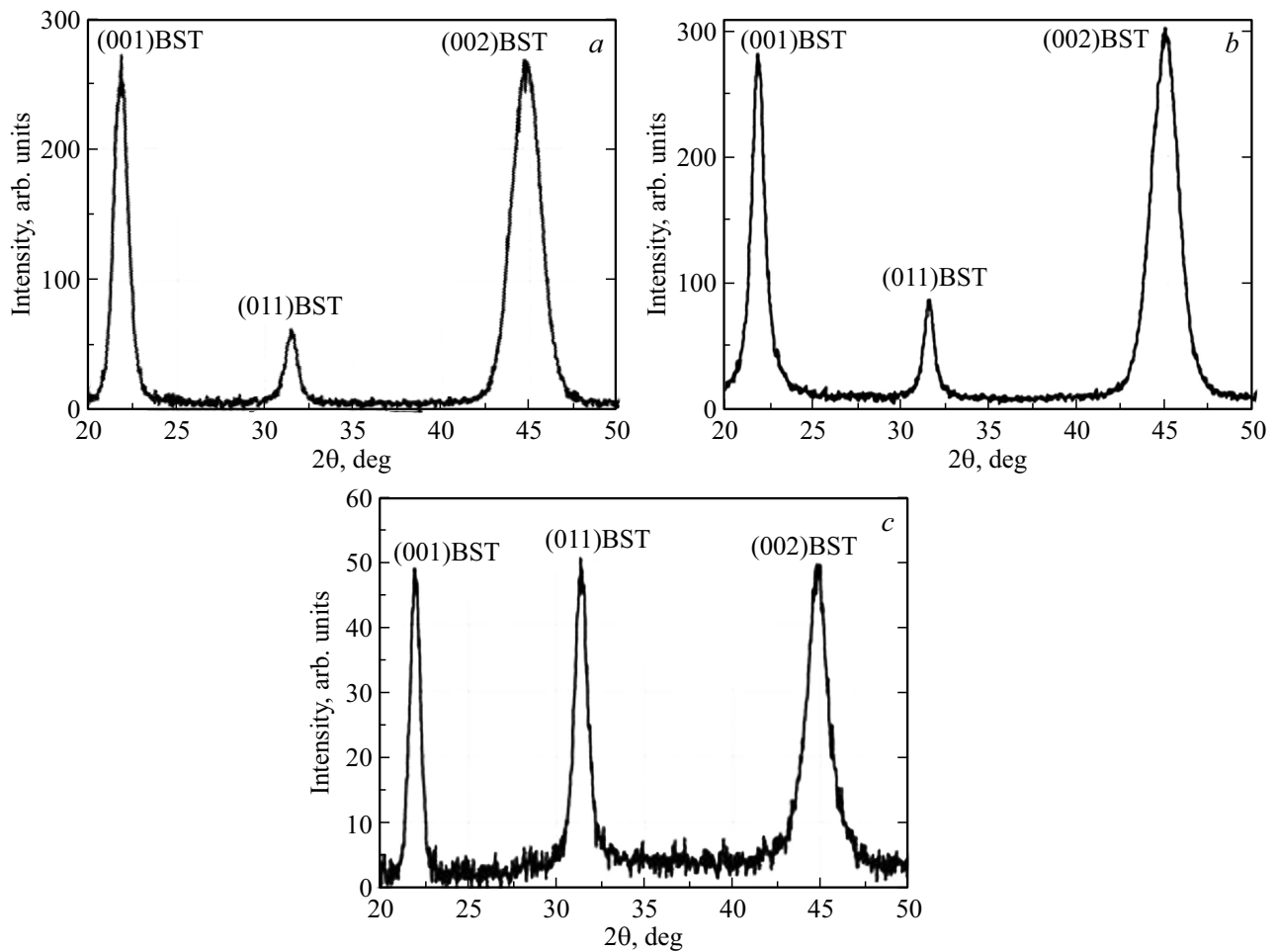


Figure 2. Diffraction patterns of BST films on a silicon substrate: *a* — Si (p-type), film thickness is 300 nm; *b* — Si (n-type), film thickness is 375 nm; *c* — Si (p-type) film thickness is 50 nm.

Table 1. Binding energies Ba4*d*-, Sr3*d*-, Ti2*p*-, and O1*s*-levels (in eV) in BST films of different thicknesses

Film thicknesses BaSrTiO ₃ , nm	Ba4 <i>d</i>		Sr3 <i>d</i>		Ti2 <i>p</i>		O1 <i>s</i>		
	5/2	3/2	3/2	1/2	3/2	1/2	A	B	C
0.83	89.6	92.2	133.6	135.4	458.75	464.5	529.5	530.4	532.3
1.66	89.7	92.3	133.6	135.4	458.75	464.55	529.8	530.45	532.45
2.49	89.3	92.0	133.2	135.0	458.37	464.37	529.85	531.42	532.45
7.5	89.4	92.0	133.2	135.0	458.25	464.07	529.6	531.4	532.42
300–375	87.80	90.4	132.3	134.1	457.2	462.80	528.9	531.0	532.7

are perpendicular to the substrate plane. The volume percentage of BST crystallites with the [001] orientation in a thin film is 79%, and the volume percentage of BST crystallites with the [011] orientation is 21%.

For a thin film, lattice constants of BST lattice cells along the normal direction to the substrate surface were also determined from the angular positions of the (002) lines, which turned out to be equal to $c = 0.4041$ nm. Compared to the bulk material, the lattice constants of this film are increased; therefore, thin BST films also contain compressive stresses in the plane of the substrate.

2.3. State of the surface of BST films according to X-ray photoelectron spectra

Figure 3 shows the Ba4*d*-, Sr3*d*-, Ti2*p*-, and O1*s*-spectra of a 300 nm thick BST film on Si(p)-substrate, and Table 1 shows binding energies of Ba4*d*-, Sr3*d*-, Ti2*p*-, and O1*s*-levels (in eV) in BST films of different thicknesses. It can be seen from Figure 3 that the X-ray photoelectron spectra of Ba4*d* of all studied samples have two components identified as Ba_{BST} and Ba_{surf} by us. The origin of the Ba_{surf} component has been studied by a number of

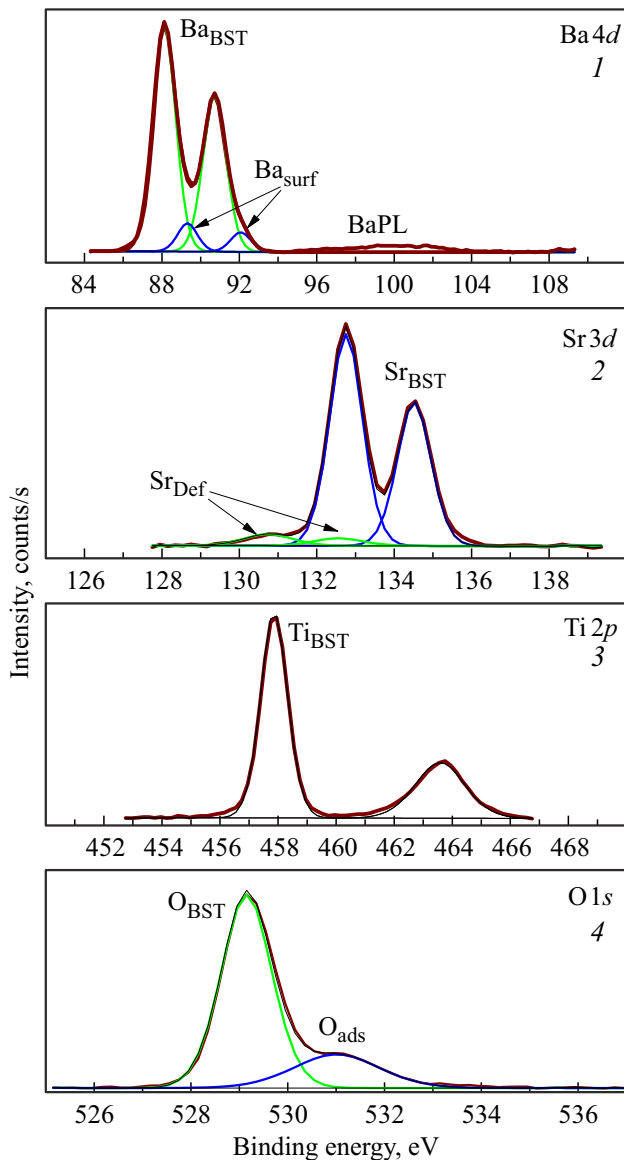


Figure 3. X-ray photoelectron $Ba4d$ -, $Sr3d$ -, $Ti2p$ -, and $O1s$ -spectra of a 300 nm thick BST film on a $Si(p)$ -substrate. $BaPL$ is plasmon peak from the $Ba4d$ -line.

authors [22–24], including us [22] within the study of single-crystal $BaTiO_3$. Ba ions located in the surface layer have a smaller number of oxygen ions in their immediate environment. When interacting with oxygen, the internal levels of the $Ba4d_{5/2,3/2}$ line experience a negative shift, i.e. a shift towards lower binding energies [24,25]. Therefore, the components of barium ions located closer to the surface have more energy.

Due to the replacement of Ba ions with strontium ions in the BST lattice, the surface components should appear in the $Ba4d$ - and $Sr3d$ -spectra in the same places [22].

The X-ray photoelectron spectrum of $Sr3d$ (Figure 3, panel 2) has two components, which we have identified in the same way as in the case of the $Ba4d$ -spectrum. The Sr_{BST} component, depending on the film thickness,

varies in a range of $133.6 \div 132.3$ eV, decreasing as the film thickness increases. This binding energy is well consistent with the binding energy of the $Sr3d_{5/2}$ level in the $SrTiO_3$ film with a perovskite structure, which is equal to 132.5 eV [26]. The Sr_{Def} component, which has a lower binding energy, appears in the spectrum of the film if there is an excess number of oxygen atoms surrounding the strontium atoms compared to the bulk material.

The X-ray photoelectron spectrum of $O1s$, presented in Figure 3 (panel 4) has two components, and in the general case (see Table 1) it has three components. The most intense of them has a binding energy, which is in the range of 529.8–528.8 eV according to Table 1. Its energy, as well as that for the $Ba4d$ - and $Sr3d$ -lines of barium and strontium atoms built into the BST lattice, decreases with increasing film thickness. This value is well consistent with the data on the position of the $O1s$ -line in single-crystal samples of $SrTiO_3$ (528.8) and $BaTiO_3$ (528.9) [27–32]. A, B, C components have energies in the intervals of $529.5 \div 529.8$, $530.4–531.4$, and $532.3–532.7$ eV, respectively. High-energy „tails“ with an energy of $530.4 \div 531.4$ eV are observed in the $O1s$ -spectra of various perovskite-like materials [27–32]. We attribute the C component with a binding energy in the range of $532.3–532.7$ eV to oxygen OH-groups or to oxygen of water vapor on the surface of the films [27,28].

The X-ray photoelectron spectrum of the $Ti2p$ thick film shown in Figure 3 (panel 3) has only two peaks due to the spin-orbit splitting of the $Ti2p_{3/2,1/2}$ -levels. We assign the spectrum of $Ti2p$ to the BST structure [26]. The energy position of the $Ti2p_{3/2}$ -peak changes from 458.7 to 457.3 eV when switching-over from thin to thick films.

3. Results and discussion

3.1. Evolution of $Si2p$ -spectra with changes in film thickness

The electronic structure of the Si/SiO_2 interface is the subject of intensive research using various methods. In particular, surface differential reflectivity (SDR) spectroscopy [33]; modulated capacitance spectroscopy [34]; ultraviolet photoelectron spectroscopy (ARXPS) [35]; X-ray photoelectron spectroscopy [36–38] are used. According to this data, the Si/SiO_2 interface (including the clean silicon surface) contains defects that create surface states in the band gap [34,36]. These defects are caused by broken silicon bonds on the surface. Their density, according to various estimates, is up to $8 \cdot 10^{14} \text{ cm}^{-2}$ [38]. When thermal oxide forms on silicon, the density of surface states decreases by two orders of magnitude down to $\sim 10^{12} \text{ cm}^{-2}$.

Figure 4 shows $Ba4d$ and $Si2p$ X-ray photoelectron spectra in an energy range of $82 \div 112$ eV, taken from the surface of cleaned silicon and the surfaces of BST films with a thickness from 0.6 to 7.5 nm. The profiles of $Si2p$ -spectra from the surface of all BST films on a silicon substrate exhibit Si–Si bonds around 99.2 eV. Due to the fact that

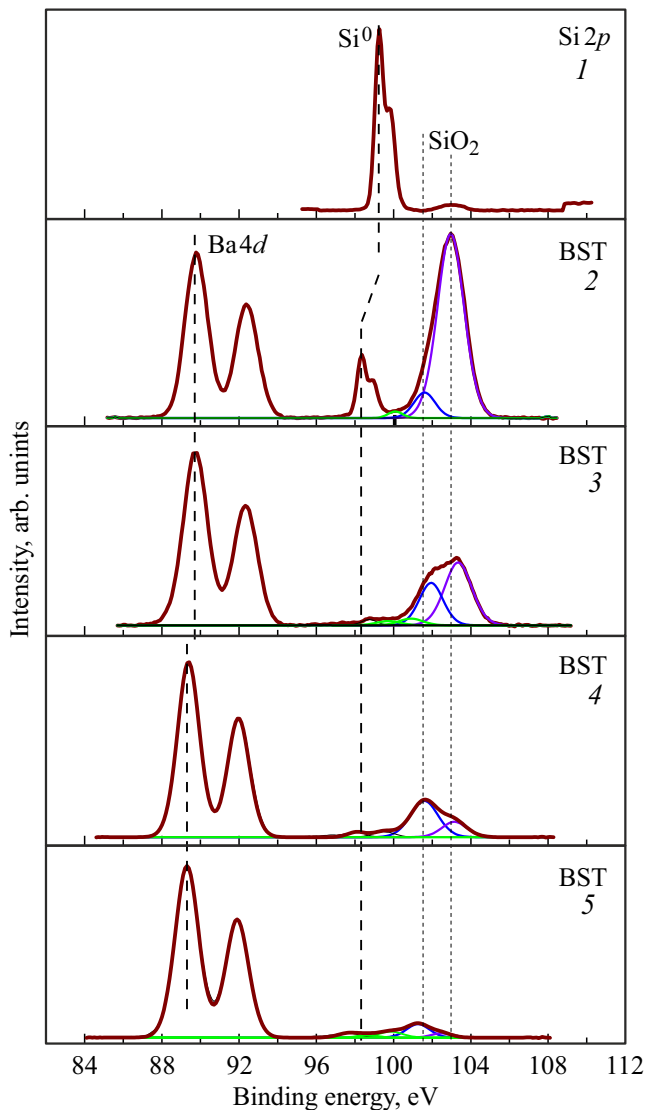


Figure 4. Changes in the intensities of Ba4d and Si2p X-ray photoelectron spectra with increasing thickness of the BST film on a Si(100) p-type substrate: 1 — Si-p(100)-substrate after cleaning in HF and washing in deionized water; 2 — BST film with a thickness of 0.6 nm; 3 — BST film with a thickness of 1.6 nm; 4 — BST film with a thickness of 2.5 nm; 5 — BST film with a thickness of 7.5 nm.

the depth of analysis by X-ray photoelectron spectroscopy is approximately equal to 3λ [39] (λ being mean electron free path), it can be assumed that the greatest thickness of the studied BST film, equal to 7.5 nm, does not exceed three mean free paths of an electron in this material excited from the Si2p-levels of the silicon substrate. Panel 1 shows the Si2p X-ray photoelectron spectrum with a binding energy of 99.2 eV, which corresponds to Si⁰ silicon [40]. At a distance of 3.7 eV from it there is a small peak, which we attributed to Si2p-silicon of Si⁴⁺ in the SiO₂ oxide [37]. As the thickness of the BST film increases, the intensity ratio of the Ba4d/Si2p-spectra increases. And the decrease in the intensity of the electronic Si2p-line with increasing

d_{BST} distance from the Si/SiO₂ interface, due to the effect of the exponential factor $\exp(-d_{\text{BST}}/\lambda)$, is accompanied by a change in its profile. The latter indicates a change in the chemical state of silicon at the Si/BST interface during the formation of the crystal structure and chemical bonds corresponding to BST. Figure 5 shows Si2p-spectra of BST films of different thicknesses on silicon substrates. Column „a“ shows Si2p-spectra of silicon substrates with p-conductivity, and column „b“ shows silicon substrates with n-conductivity. Energy positions of maximum of the Si2p-line of cleaned surfaces of silicon substrates with p-conductivity and n-conductivity in Figure 5, a (panel 1) and Figure 5, b (panel 1) are approximately the same within the accuracy of binding energy measurements, i.e. 99.2 ± 0.1 and 99.4 ± 0.1 eV, respectively. In X-ray photoelectron spectroscopy, the binding energy is measured relative to the energy of the Fermi level, located within the band gap in the case of semiconductors [41]. Typically, for silicon with n-conductivity, depending on the doping level, it is located closer to the conduction band, and for a sample with p-conductivity, it is closer to the upper edge of the valence band. Therefore, the binding energy of the same level in a semiconductor with n-conductivity is usually slightly higher than that in a material with p-conductivity. This is qualitatively consistent with our data for specific silicon samples. As it follows from Figure 5, when a BST film is deposited on silicon substrates with different types of conductivity, in both cases the Fermi level in the conduction band drops by approximately 1 eV (in the case of a semiconductor with n-conductivity the drop is ~ 1.1 eV, for a substrate with p-conductivity it is slightly lower — ~ 0.9 eV). Taking into account that the band gap of silicon is 1.12 eV [42], this means that in the initial state of the silicon substrate with n-conductivity before deposition the Fermi level was exactly at the edge of the band gap, and in a substrate with p-conductivity it was 0.2 eV lower. Even with the deposition of a BST layer with a thickness of 0.8 nm, the Fermi level in the band gap of both substrates drops to the edge of the valence band. The fine structure of the Si2p-spectra in Figure 5 on the panels on the left and right characterizes silicon bonds of Si—Si, Si—O (here O stands for the oxygen atom belonging to the intermediate oxide of SiO_x and SiO₂), Si—O_{BST} types (here O_{BST} stands for the oxygen atom binding the silicon atom of the substrate and one of the atoms of the BST structure).

In the case of a BST layer with a thickness of 0.8 nm, the percentage of Si—Si bonds in Figure 5 on the left (panel 2) in the total number of bonds of Si⁰ silicon atoms is about 13%, the percentage of the number of silicon atoms in the oxidation state typical for the SiO₂ structure is about 78%, and the percentage of silicon atoms associated with atoms of the BST structure (the Si—BST component in Figure 5) is about 7%. The percentage of silicon atoms in the state of intermediate oxidation (SiO_x component in Figure 5) is about 2%. With increasing layer thickness, these percentages change and for a layer with a thickness of 7.5 nm (Figure 5, left, panel 5) they are as follows: the percentage of Si—Si bonds increases to 18%; the percentage

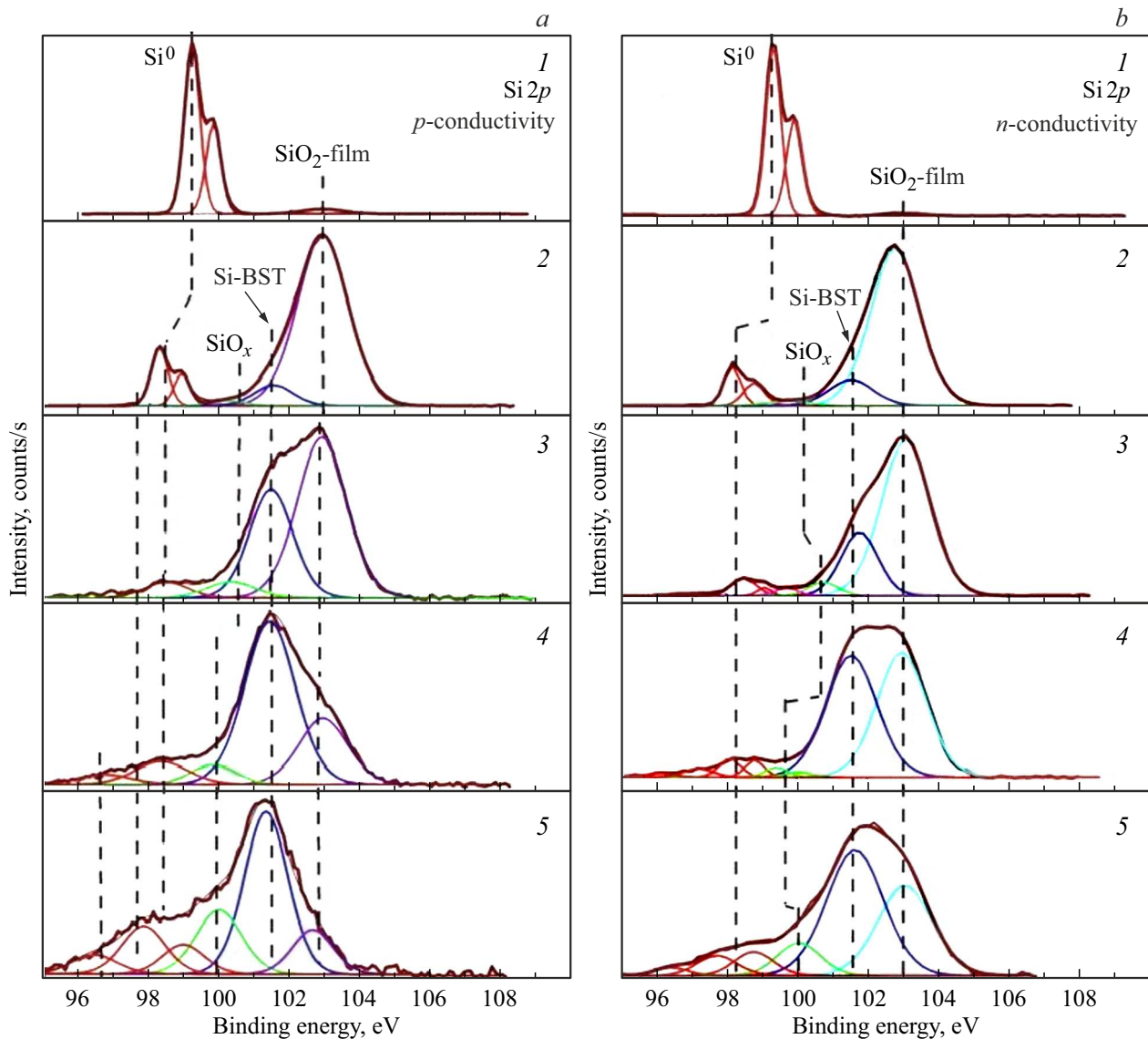


Figure 5. Evolution of X-ray photoelectron spectra of Si2p with increasing thickness of the BST film on the Si-p(100) substrate: 1 — Si-p(100)-substrate after cleaning in HF; 2 — BST film with a thickness of 0.83 nm; 3 — BST film with a thickness of 1.66 nm; 4 — BST film with a thickness of 2.49 nm; 5 — BST film with a thickness of 7.5 nm.

of silicon atoms belonging to SiO_2 decreases down to 12%; the percentage of silicon atoms in intermediate oxidation states becomes equal to 24%, and the percentage of silicon atoms associated with atoms of the BST structure increases to 46%. In this regard, it should be noted that the chemical state of silicon atoms at the Si/BST interface changes approximately equally with increasing BST layer thickness for substrates of p-type and n-type conductivities.

Thus, the mechanism of BST growth, at least to a thickness of 7.5 nm, ensures at the Si/BST interface a constant increase in the percentages of the chemical state of silicon atoms involved in establishing bonds with the atoms of the BST structure, a decrease in the percentages of silicon atoms in the composition of oxides with the chemical formula of SiO_2 . The energy position of the silicon component in the intermediate oxidation state of SiO_x for both substrates on

the panels 5 is shifted relative to the energy of the Si2 line on the panel 2 by approximately 1.8 eV. According to [37,38], these components can be attributed to Si^{2+} silicon. The Si2p-spectra of both substrates (with p-type and n-type conductivity) are characterized by a shift of the components related to Si–Si fragments towards lower binding energies with an increase in the thickness of the BST layer for the initial structure of the surface of silicon substrates before deposition. This shift, if measured along the low-energy edge of the Si2p-spectrum, is 2.4 eV for a substrate with n-conductivity and 3.3 eV for a substrate with p-conductivity. The presence of these components in the X-ray photoelectron spectrum of Si2p after the formation of a BST layer with a thickness of up to 7.5 nm on a silicon substrate is not clear. In [37], within the study of the Si/ SiO_2 interface, the presence of silicon atoms in the

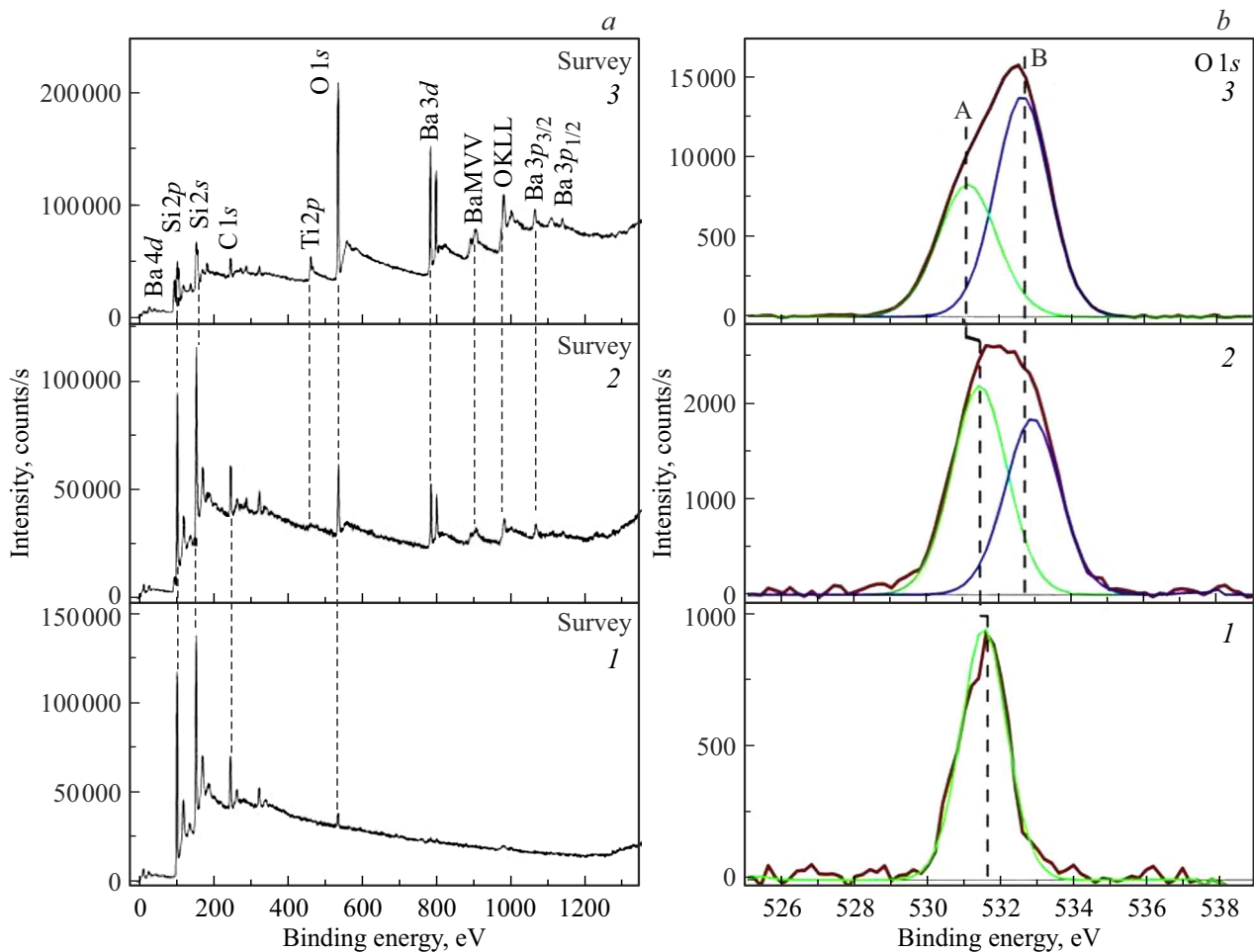


Figure 6. X-ray photoelectron spectra: overview (panel *a*) and O1s-spectra (panel *b*), recorded at points A, B, C on the generatrix of the cones located at heights $\sim 0 \text{ \AA}$ (Figure 6.1, *a, b*), $\sim 3 \text{ \AA}$ (Figure 6.2, *a, b*), $\sim 6 \text{ \AA}$ (Figure 6.3, *a, b*), respectively, relative to the crater bottom.

oxidation state Si^{4+} , Si^{3+} , Si^{2+} , and Si^{1+} was discovered at the Si/SiO₂ interface, which actually means the appearance at the interface of stoichiometric SiO₂ and fragments with excess silicon of SiO₃Si, Si₂O₂Si, and Si₃OSi, respectively. Due to the fact that we have the Si^{2+} silicon component in the valence state at the Si/BST interface, we can assume the presence of structures or defects enriched with silicon of the O₃≡Si–Si≡O₃ or Si₂O₂Si type at the interface. Some of the oxygen atoms in these formulas may be atoms that bind the substrate and the structure of the BST coating.

3.2. X-ray photoelectron spectra of the Si/BST interface of a wedge-shaped profile

For a more detailed examination of the depth structure of the Si/BST interface, we etched a crater with a depth of 2.5 and a diameter of 5 mm in a 2.5 nm thick film using sputtering with Ar⁺ ions. The walls of the conical crater were located at a very small angle α with respect to the plane of the substrate, the tangent of which was $\sim 10^{-6}$. The crater walls, inclined at a very small angle to the surface, are actually an implementation of the „wedge method“ known

in the literature on X-ray spectral microanalysis, which improves the spatial resolution of the method [43]. The diameter of the X-ray probe was $250 \mu\text{m}$, i.e. only 0.05 of the crater diameter. The X-ray photoelectron spectra were recorded at points A, B, C, D on the generatrix of the crater cone, shifted relative to the center of the crater (point A) horizontally by $309 \mu\text{m}$ (point B), $601 \mu\text{m}$ (point C), and $1076 \mu\text{m}$ (point D). Assuming the generatrix of the ion etching crater is straight, a horizontal shift by the above distances leads to an increase in the area irradiated by the X-ray probe by values of $\sim 3 \text{ \AA}$ (point B), 6 \AA (point C), and $\sim 10 \text{ \AA}$ (point D).

From the center of the crater (point A), overview spectra were recorded, as well as Si2p-, Ba4d-, Sr3d-, Ti2p-, and O1s-photoelectron X-ray spectra presented in Figures 6, *a, b* and Figure 7, *a, b, c* in the first panels were recorded separately. Analysis of the overview X-ray photoelectron spectrum on the panel „*a*“ in Figure 6.1 shows that the surface of the silicon substrate in the center of the crater was almost cleared of BST film atoms: the overview spectrum contains only lines of silicon, argon, and oxygen. Ar2p- and Ar2s-spectra were recorded from argon atoms embedded

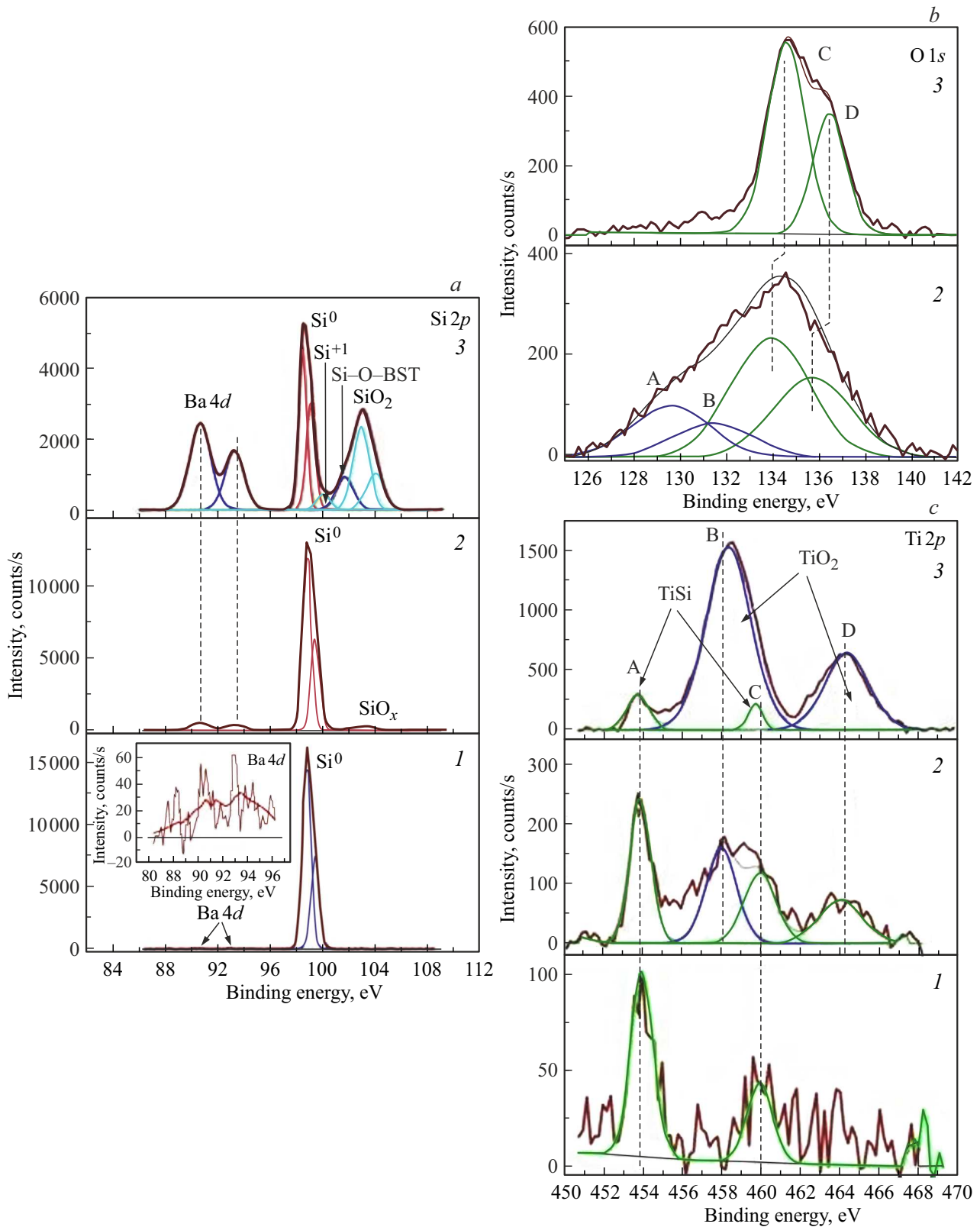


Figure 7. X-ray photoelectron $Ba4d$ -, $Si2p$ -, $Sr3d$ -, and $Ti2p$ -spectra: recorded at points A, B, C on the generatrix of the cone located at heights of $\sim 0\ \text{\AA}$ (Figure 7.1, a, c), $\sim 3\ \text{\AA}$ (Figure 7.2, a, b, c), $6\ \text{\AA}$ (Figure 7.3, a, b, c), respectively, relative to the crater bottom.

in the silicon substrate during ion etching. The energy position of the $O1s$ electron line in Figure 6.1, *b* was equal to 531.3 eV, which corresponds to adsorbed oxygen [25–30] on the etched silicon surface. The energy position of the $Ti2p_{3,2}$ -line (peak A in Figure 7, *c*), equal to 453.9 ± 0.1 eV, corresponded to metallic titanium [44]. This is only 0.3 eV greater than the binding energy of titanium compounds with silicon, $TiSi$ or $TiSi_2$. Therefore, it can be assumed that these titanium atoms can be chemically bonded to the silicon atoms closest to them. As follows from the overview spectra in Figures 6.1, *a*, 6.2, *a*, 6.3, *a*, recorded at points A, B, and C, located at heights of ~ 0 Å (Figure 6.1, *a, b*), ~ 3 Å (Figures 6.2, *a, b*), 6 Å (Figure 6.3, *a, b*), respectively, relative to the crater bottom, with an increase in the analyzed thicknesses, the intensities of the lines of elements related to the BST film increase and the intensities of the $Si2p$ -lines of the substrate decrease. The $Si2p$ -lines in Figure 7.3, *a* evolve to a profile typical for the Si/BST interface, similar to the profiles of the $Si2p$ -spectra in Fig 5, *a, b* already discussed above. It can be noted that the Si/BST interface for a BST film with a thickness of ~ 6 Å is already fully formed with all the features of the chemical bonds at the interface discussed above. The same conclusion follows from the consideration of the energy position of the $O1s$ -, $Ba4d$ -, $Sr3d$ -, and $Ti2p$ -spectra presented in Figures 6.3, *b*, 7.3, *a*, 7.3, *b* and 7.3, *c*, respectively. The energy position of the $Ba4d$ -, $Sr3d$ - and B and C components of the $Ti2p$ -spectra and their profiles are typical for fully formed $Ba(Sr)-O$ - and $Ti-O$ -layers of the BST structure. The exception is peak A in the profile of the $Ti2p$ -spectrum in Figures 7.1, *c*, 7.2, *c*, and 7.3, *c*. As noted above, this peak refers to the chemical state of titanium close to titanium silicide. As can be seen from Figure 7, *c* this peak decreases with increasing thickness of the BST film, indicating that titanium atoms of this type belong to the Si/BST interface.

From the point of view of the features of the chemical bond, the profiles of $Sr3d$ - and $Ti2p$ -spectra in Figure 7.2 in panels *b* and *c*, respectively, are interesting. They refer to a layer with a thickness corresponding to the height of the spectra in region B. It can be seen from Figure 7.2, *b* and *c* that the $Sr3d$ - and $Ti2p$ -spectra contain low-energy components (A, B for the $Sr3d$ -spectrum) and (A, C for the $Ti2p$ -spectrum) and components with higher binding energy (C, D for the $Sr3d$ -spectrum) and (B, D for the $Ti2p$ -spectrum). We attribute the low-energy components in the case of the $Ti2p$ -spectrum to the titanium atoms located directly in the silicon layer near the interface, and the second components in the $Sr3d$ - and $Ti2p$ -spectra are attributed to the strontium and titanium atoms embedded in the BST lattice.

In the above, we have identified the low-energy components A and B in the $Sr3d$ -spectrum of the thick BST film in Figure 3, and we attributed them to the strontium atoms surrounded by a large number of oxygen atoms, which occur in the BST structure, i.e. to a defective structure. At the Si/BST interface, as we discussed above, there are oxygen atoms that are not embedded in the BST lattice, but with which strontium atoms can also be associated. Therefore,

we attribute the low-energy components A and B in the $Sr3d$ -spectra to strontium atoms at the Si/BST interface.

The incorporation of strontium atoms into the upper layer of silicon, according to a number of authors, is facilitated by the structure of the upper $Si(001)$ layers of the surface of single-crystal silicon [14,45–47]. It is generally accepted that the $Si(001)$ surface consists of dimers, which constitute the (2×1) basic structural unit of the reconstructed surface [46,47]. The 2×1 superlattice on the $Si(001)$ surface is observed at room temperature. The surface contains significant subsurface distortions extending several layers deep [14,47]. Currently, there are two models of the upper $Si(001)$ layer that are equivalent to each other from the point of view of the evidential base: symmetrical and asymmetrical models [45]. In the case of the implementation of the asymmetric dimer model of $Si(2 \times 1)$ of the reconstructed surface layer, the first layer is represented by dimers consisting of two silicon atoms, one of which is shifted in depth [45]. According to theoretical and experimental data [46,48,49], the energy levels of the lower silicon atom in the dimer are shifted towards lower binding energies by a value of approximately from 0.6 to 1 eV. Thus, the decrease in the binding energy of the $Sr3d$ - and $Ti2p$ -levels for some strontium and titanium atoms, which we recorded at the interface, within the framework of the asymmetric model of the $Si(001)$ silicon surface can be explained by the incorporation of Sr and Ti atoms into free places in reconstructed surface of $Si(001)$ (2×1) enlarged as compared to the volume of the lattice cell. In [50], it was established that when barium and strontium atoms are deposited onto a $Si(001)$ substrate within the framework of the symmetric dimer model of the $Si(001)$ (2×1) surface structure the Ba and Sr atoms can occupy sites of the same type (2×1) $Ba/Si(001)$ and (2×1) $Sr/Si(001)$, i.e. free places in the enlarged cell of (2×1) $Si(001)$. At the same time, the authors of [50] have experimentally discovered that adatoms of the (2×1) $Ba/Si(001)$ phase are located at a height 0.14 Å higher than adatoms of the (2×1) $Sr/Si(001)$. The authors of [50] explained this fact by the difference in the sizes of the ionic radii of barium and strontium. A little earlier, the authors of [13] used photoelectron spectroscopy to study the growth of a coating of Sr atoms with a thickness from 0 to 1 monolayer on a single-crystal surface of n-type $Si(001)$. According to the interpretation of the authors of [13], which they performed within the framework of the asymmetric dimer model of the $Si(100)$ (2×1) surface, the Sr atom, interacting with the lower Si atom in the dimer, introduces a charge into this atom, lowering the binding energy so that it becomes close to the binding energy of the upper silicon atom. However, at the same time, their experimental data shows that the layer of Sr atoms forms a sharp interface on top of the $Si(001)$ without removing the top surface atoms of the Si dimer [13]. Thus, regardless of the models within which the results are interpreted, when barium or strontium atoms are deposited onto a single-crystal $Si(100)$ surface, these atoms occupy positions within one monolayer in an enlarged surface as compared to the lattice cell volume,

Table 2. Ratios $(I_{Ba}/\sigma_{Ba} + I_{Sr}/\sigma_{Sr})/(I_{Ti}/\sigma_{Ti})$ and $Ba_{1-x}Sr_xTiO_y$ for different BST film thicknesses corresponding to recording points A, B, C, and D on the generatrix of the crater cone

Region of recording	$(I_{Ba}/\sigma_{Ba} + I_{Sr}/\sigma_{Sr})/(I_{Ti}/\sigma_{Ti})$	$Ba_{1-x}Sr_xTiO_y$
A	0.29	$Ba_{0.09}Sr_{0.7}Ti_{0.305}O_{4.6}$
B	3.11	$Ba_{0.28}Sr_{0.675}Ti_{0.305}O_{3.73}$
C	1.21	$Ba_{0.515}Sr_{0.22}Ti_{0.61}O_{3.66}$
D	0.78	$Ba_{0.49}Sr_{0.145}Ti_{0.81}O_{3.55}$

forming a sharp boundary. In [15,51], the Si(100)/SrTiO₃ interface was studied using high-resolution transmission electron microscopy and X-ray photoelectron spectroscopy. According to these studies, the SrTiO₃/Si interface is sharp. The SrTiO₃ film interacts with the Si(100) (2 × 1) surface through strontium atoms according to the models considered in [13,51]. And the X-ray photoelectron spectroscopy data supports the conclusion that the bond with the substrate occurs through strontium atoms, which form silicates with silicon atoms [51]. At the same time, the authors of [15] believe that the interface most likely consists of Si bound to O in SrTiO₃.

By analyzing the chemical state and intensity ratio of the Ba4*d*-, Si2*p*-, Sr3*d*- and Ti2*p*-lines in Figures 6 and 7, a conclusion can be made that these spectra indicate, at least, the presence of strontium and titanium atoms directly in the body of the silicon substrate at the interface itself and in two monolayers of strontium, barium, and titanium atoms associated with oxygen, i.e. Ba(Sr)–O and Ti–O located above. However, qualitative analysis does not allow determining the order of the layers. Table 2 shows the ratios of $(I_{Ba}/\sigma_{Ba} + I_{Sr}/\sigma_{Sr})/(I_{Ti}/\sigma_{Ti})$ for four recording points A, B, C, D and the formal elemental composition of $Ba_{1-x}Sr_xTiO_y$ corresponding to these thicknesses.

The I_{Ba} , I_{Sr} , I_{Ti} and σ_{Ba} , σ_{Sr} , σ_{Ti} notations refer to the intensities of the X-ray photoelectron lines of Ba4*d*, Sr3*d*, Ti2*p* and factors of the elemental sensitivity upon excitation of these lines according to Wagner, respectively [52]. Analysis of the data in Table 2 allows making a confident conclusion that the layer rising above the interface and represented by the spectral recording region B with the ratio of $(I_{Ba}/\sigma_{Ba} + I_{Sr}/\sigma_{Sr})/(I_{Ti}/\sigma_{Ti}) = 3.11$ is the Ba(Sr)–O layer. Records at higher points C and D demonstrate a consistent increase in the content of titanium atoms (Ti–O layer), as well as barium and strontium atoms, approaching its content in the thick BST film.

The experimental material discussed above is well consistent with the concepts of a sharp interface discussed in [15,51] for the case of deposition of a SrTiO₃ strontium titanate film on a single-crystal Si(001) substrate.

Combining the results obtained from Figures 3, 6 and 7 for the analysis of chemical bonds at the Si/BST interface, a conclusion can be made that 46% of silicon atoms are bound to the BST structure through oxygen atoms belonging to the BST structure. Some of the strontium and

titanium atoms of the deposited BST film are located in the uppermost layer of the dimerized Si(001) (2 × 1) structure alternating with silicon atoms. They can form chemical bonds with silicon atoms. In this respect, our results are consistent both with the conclusions of [52] and with the assumptions of [15].

4. Conclusion

Single-crystal films of $Ba_{0.71}Sr_{0.27}Ti_{1.03}O_{2.99}$ were formed on Si(001) silicon substrates from p-type and n-type silicon. The X-ray diffraction of the films showed that the volume percentage of BST crystallites with the [001] orientation is 96% for the n-type Si substrate and 97% for the p-type Si substrate. The volume percentage of BST crystallites with the [011] orientation is 4% for the n-type Si substrate and 3% for the p-type Si substrate.

The X-ray photoelectron spectroscopy data on the chemical state of the Si(001)/BST interface showed the following: 46% of silicon atoms at the interface are bound with oxygen belonging to the BST structure; 18% silicon atoms belong to the SiO₂ layer. At the Si(001)/BST interface, O₃≡Si–Si≡O₃ defects caused by the presence of one oxygen vacancy at the interface, and defects of the O₃≡Si–Si–Si≡O₃ type caused by the presence of an oxygen vacancy were detected.

The Si/BST interface is sharp and at a thickness of ~ 6 Å is already fully formed. The adhesion of a BST film to a silicon substrate is implemented in a combined manner: a — through chemical bonds of surface silicon atoms with oxygen of the BST structure; b — through titanium and strontium atoms chemically bound to silicon at the interface and simultaneously to oxygen in the BST structure.

Funding

The study was supported financially by the Ministry of Science and Higher Education of the Russian Federation (State assignment in the field of scientific activity for 2023 No. FENW-2023-0014 and State assignment of the Southern Research Center of the Russian Academy of Sciences for the project No. 122020100294-9).

Conflict of interest

The authors declare that they have no conflict of interest.

References

- [1] S.Y. Hou, J. Kwo, R.K. Watts, J.Y. Cheng, D.K. Fork. Appl. Phys. Lett. **67**, 1387 (1995).
- [2] D. Ivanov, M. Caron, L. Ouellet, S. Blain, N. Hendric, J. Currie. J. Appl. Phys. **77**, 2666 (1995).
- [3] B. Acikel, T.R. Taylor, P.J. Hausen, J.S. Speck, R.A. York. IEEE Microwave Wireless Comp. Lett. **12**, 7, 237 (2002).
- [4] P.K. Petrov, N.M. Alford, S. Gevorgyan. Meas. Sci. Technol. **16**, 583 (2005).

- [5] C.M. Carlson, T.V. Rivkin, P.A. Parilla, J.D. Perkins, D.S. Ginley, A.B. Kozyrev, V. N. Oshadchy, A.S. Pavlov. *Appl. Phys. Lett.* **76**, 1920 (2000).
- [6] C.M. Carlson, T.V. Rivkin, P.A. Parilla, J.D. Perkins, D.S. Ginley, A.B. Kozyrev, V.N. Oshadchy, A.S. Pavlov, A. Golovkov, M. Sugak, D. Kalinikos, L.C. Sengupta, L. Chiu, X. Zhang, Y. Zhu, S. Sengupta. *Mater. Res. Soc. Symp. Proc.* **603**, 15 (2000).
- [7] W.J. Kim, W. Chang, S.B. Qadri, J.M. Pond, S.W. Kirchoefer, D.B. Chrisey, J.S. Horwitz. *Appl. Phys. Lett.* **76**, 1185 (2000).
- [8] B.H. Hoerman, B.M. Nichols, B.W. Wessels. *Phys. Rev. B: Condens. Matter* **65**, 224110 (2002).
- [9] A. Kumar, S.G. Manavalan. *Surf. Coat. Technol.* **198**, 406 (2005).
- [10] S.H. Kim, C.E. Kim, Y.J. Oh. *Thin Solid Films* **305**, 32 (1997).
- [11] A.H. Mueller, N.A. Suvorova, E.A. Irene, O. Auciello, J.A. Schultz. *Appl. Phys. Lett.* **80**, 3796 (2002).
- [12] R.F. Pinizzotto, E.G. Jacobs, H. Yang, S.R. Summerfelt, B.E. Gnade. *Mater. Res. Soc. Symp. Proc.* **243**, 1992 (1991).
- [13] A. Herrera-Gómez, F.S. Aguirre-Tostado, Y. Sun, P. Pianetta, Z. Yu, D. Marshall, R. Droopad, W.E. Spicer. *J. Appl. Phys.* **90**, 12, 6070 (2001).
- [14] R.A. McKee, F.J. Walker, M.F. Chisholm. *Phys. Rev. Lett.* **81**, 14, 3014 (1998).
- [15] G.Y. Yang, J.M. FINDER, J. Wang, Z.L. Wang, Z. Yu, J. Ramdani, R. Droopad, K.W. Eisenbeiser, R. Ramesh. *J. Mater. Res.* **17**, 1, 204 (2002).
- [16] V.M. Mukhortov, Yu.I. Yuzyuk, *Geterostruktury na osnove nanorazmernykh segnetoelektricheskikh plynok: poluchenie, svoystva i primenenie. Izd-vo YuNTs RAN, Rostov-na-Donu* (2008). 224 s. (in Russian).
- [17] V.M. Mukhortov, Yu.I. Golovko, G.N. Tolmachev, A.I. Maschenko, *ZhTF* **69**, 12, 87 (1999). (in Russian).
- [18] L. Ley, S.P. Kowalczyk, R.A. Pollak, D.A. Shirley. *Phys. Rev. Lett.* **29**, 1088 (1972).
- [19] E. Walker, C.P. Lund, P. Jennings, J.C.L. Cornish, C. Klauber, G. Hefter. *Appl. Surf. Sci.* **222**, 13 (2004).
- [20] S.Y. Wang, B.L. Cheng, Can Wang, T.W. Button, S.Y. Dai, K.J. Jin, H.B. Lu, Y.L. Zhou, Z.H. Chen, G.Z. Yang. *J. Phys. D* **39**, 979 (2006).
- [21] W.D. Mesquita, M.C. de Oliveira, M. Assis, R.A.P. Ribeiro, A.C. Eduardo, M.D. Teodoro, G.E. Marques, M.G. Júnior, E. Longo, M.F.C. Gurgel. *Mater. Res. Bull.* **143**, 111442 (2021).
- [22] A.T. Kozakov, A.V. Nikolsky, K.A. Guglev, E.M. Panchenko, *Izv. RAN, Ser. fiz.* **76**, 1, 138 (2012). (in Russian).
- [23] L.T. Hudson, R.L. Kurtz, S.V. Robey, D. Temple, R.L. Stockbauer. *Phys. Rev. B* **47**, 3, 1174 (1993).
- [24] L.T. Hudson, R.L. Kurtz, S.V. Robey, D. Temple, R.L. Stockbauer. *Phys. Rev. B* **47**, 16, 10832 (1993).
- [25] K. Jacobi, C. Astaldi, B. Frick, P. Ceng. *Phys. Rev. B* **36**, 6, 3079 (1987).
- [26] D. Ehre, H. Cohen, V. Lyahovitskaya, I. Lubomirsky. *Phys. Rev. B* **77**, 184106 (2008).
- [27] A.G. Kochur, A.T. Kozakov, A.V. Nikolskii, K.A. Googlev, A.V. Pavlenko, I.A. Verbenko, L.A. Reznichenko, T.I. Krasnenko. *J. Electron Spectrosc. Rel. Phenom.* **185**, 175 (2012).
- [28] A.T. Kozakov, A.G. Kochur, L.A. Reznichenko, L.A. Shilkina, A.V. Pavlenko, A.V. Nikolskii, K.A. Googlev, V.G. Smotrakov. *J. Electron Spectrosc. Rel. Phenom.* **186**, 14 (2013).
- [29] A. Fujimori, M. Saeki, N. Kimizuka, M. Taniguchi, S. Suga. *Phys. Rev. B* **34**, 10, 7318 (1986).
- [30] E. Begreuther, S. Grafström, L.M. Eng, C. Thiele, K. Dörr. *Phys. Rev. B* **73**, 155425 (2006).
- [31] A.E. Bocquet, A. Fujimori, T. Mizokawa, T. Saitoh, H. Namatame, S. Suga, N. Kimizuka, Y. Takeda, M. Takano. *Phys. Rev. B* **45**, 1561 (1992).
- [32] T. Yamashita, P. Hayes. *Appl. Surf. Sci.* **254**, 2441 (2008).
- [33] T.D. Mishima, P.M. Lenahan, W.D. Weber. *Appl. Phys. Lett.* **76**, 3771 (2000).
- [34] J. Albohn, W. Füssel, N.D. Sinh, K. Kliefoth, W. Fuhsa. *J. Appl. Phys.* **88**, 842 (2000).
- [35] J. Halbritter. *J. Mater. Res.* **3**, 3, 506 (1988).
- [36] F.J. Grunthaler, P.J. Grunthaler, R.P. Vasquez, B.F. Lewis, J. Maserjian. *Phys. Rev. Lett.* **43**, 1683 (1979).
- [37] F.J. Himpel, F.R. McFeely, A. Taleb-Ibrahimi, J.A. Yarmoff. *Phys. Rev. B* **38**, 9, 6084 (1988).
- [38] V.A. Gritsenko, *UFN* **179**, 9, 921 (2009). (in Russian).
- [39] A. Jablonski, C.J. Powell. *Surf. Sci.* **520**, 78 (2002).
- [40] A.T. Kozakov, N. Kumar, V.G. Vlasenko, I.V. Pankov, A.A. Tsaturyan, A.A. Scryabin, A.V. Nikolskii, A.V. Nezhdanov, R.M. Smertin, V.N. Polkovnikov, N.I. Chkhalo. *Bull. Mater. Sci.* **46**, 21 (2023).
- [41] V.I. Nefedov, V.T. Cherepin, *Fizicheskie metody issledovaniya poverkhnosti tvorydykh tel, Nauka, M., (1983), 295 s.* (in Russian).
- [42] Z. Zi, *Fizika poluprovodnikovyykh priborov, Mir, M., (1984), T. 1. 456 s.* (in Russian).
- [43] *Kolichestvennyy elektronno-zondovyy mikroanaliz / Eds. V. Scott, G. Love, Mir, M., (1986), S. 352* (in Russian).
- [44] V.I. Nefedov, *Rentgenoelektronnaya spektroskopiya khimicheskikh soedineniy, Spravochnik, Khimiya, M., (1984), 256 s.* (in Russian).
- [45] A. Ramstad, G. Brocks, P.J. Kelly. *Phys. Rev. B* **51**, 20, 14504 (1995).
- [46] E. Landemark, C.J. Karlsson, Y.C. Chao, R.I.G. Uhrberg. *Phys. Rev. Lett.* **69**, 10, 1588 (1992).
- [47] R.M. Tromp, R.G. Smeenk, F.W. Saris, D.J. Chadi. *Surf. Sci.* **133**, 137 (1983).
- [48] D.H. Rich, T. Miller, T.C. Chiang. *Phys. Rev. B* **37**, 6, 3124 (1988).
- [49] G.K. Wertheim, D.M. Riffe, J.E. Rowe, P.H. Citrin. *Phys. Rev. Lett.* **67**, 1, 120 (1991).
- [50] D.M. Goodner, D.L. Marasco, A.A. Escudero, L. Cao, M.J. Bedzyk. *Phys. Rev. B* **71**, 165426 (2005).
- [51] J.H. Hao, J. Gao, Z. Wang, D.P. Yu. *Appl. Phys. Lett.* **87**, 131908 (2005).
- [52] C.D. Wagner, L.E. Davis, M.V. Zeller, J.A. Taylor, R.H. Raymond, L.H. Gale. *Sur. Interface Anal.* **3**, 211 (1981).

Translated by Y.Alekseev